

LASER MEDICINE AND BIOLOGY

https://doi.org/10.1070/QEL16383

Study of blood plasma optical properties in mice grafted with Ehrlich carcinoma in the frequency range 0.1–1.0 THz*

O.A. Smolyanskaya, O.V. Kravtsenyuk, A.V. Panchenko,
E.L. Odlyanitskiy, J.P. Guillet, O.P. Cherkasova, M.K. Khodzitsky

Abstract. **In the course of *in vitro* studies of blood of laboratory animals with progressing Ehrlich carcinoma, we have revealed the change of the blood plasma optical properties in the THz range, which can be used for developing the express diagnostics of the presence of oncological diseases. An applied software package is elaborated that allows the phantoms of biological samples having a complex structure to be numerically simulated and the parameters of the electromagnetic wave reflected from these samples in the THz frequency range to be calculated.**

Keywords: *THz time-domain spectroscopy (THz TDS), Ehrlich tumour, SHR mice line, blood plasma, finite-difference time-domain method.*

1. Introduction

The laboratory diagnostics of tumours is based on revealing the tumour-related markers, found in malignant cells and associated with their growth. These markers are macromolecules distinguished qualitatively (tumour-specific) or quantitatively (associated with tumour, but present in normal cells too). A fraction of tumour markers is secreted into blood so that their concentration can be determined in blood plasma. About two hundred compounds associated with different cancer localisations are known, but only about two dozen proteins have diagnostic significance [1, 2]. There are no tumour markers with absolute specificity (i.e., not revealed in healthy persons and in the case of benign neoplasms) and absolute sensitivity (i.e., necessarily revealed in the presence of disease and at its early stages). The developments of novel diagnostic methods and the improvement of sensitivity in the detection of oncological diseases at early stages is an urgent problem of clinical medicine.

In recent decades the development of methods for generating and detecting THz radiation has lead to significant success in the application of THz pulsed spectroscopy to the study of medical and biological objects [3]. The method allows the refractive index and absorption coefficient dispersion to be determined in one measurement, which offers the possibility of express diagnostics development of this base. Using this method, one can also determine the dispersion of the complex permittivity of the studied sample.

The major part of THz radiation absorbed by a living tissue is absorbed by water molecules [4, 5]. This is due to the fact that the water molecules form most of the hydrogen bonds both between each other and with multiple dissolved and hydrated compounds. As a result, complex dynamical chains and networks of dipoles arise, which together respond to the environment changes. The intermolecular vibrations of the macroscopic network of dipole water molecules possess their own rotational–vibrational spectrum in the THz frequency range [5]. Besides that, the slow relaxation of large aggregations formed by water molecules using hydrogen bonds cause strong intermolecular vibrations with the frequency ~1.5 THz [5]. Due to all these features, the aqueous medium is the most efficient chromophore for THz radiation.

THz pulsed spectroscopy has been successfully used for the diagnostics of oncological pathology in a number of organs and tissues [6–11]. It was shown that the optical characteristics of pathological and healthy tissue are essentially different in the THz frequency region. The methods of THz pulsed spectroscopy have been already applied to the study of blood from donors [12, 13] and animals [14]. Measurable differences in the refractive indices and absorption coefficients of whole blood and its components were revealed. The effect is most pronounced for thrombocytes [12] and erythrocytes [13]. The linear dependence of the sample absorption coefficient on the concentration of erythrocytes in blood was found in Refs [13, 14]. The authors suggested using the method of THz pulsed spectroscopy for haematocrit determination.

THz pulsed spectroscopy was shown to be applicable to the studies of blood plasma in the case of different pathologies. Thus, a negative correlation between the absorption coefficient of THz radiation and the number of erythrocytes and triglycerides in the blood of cardiosurgery department patients was observed in Ref. [15]. It was found that the significant change of the blood plasma composition in the case of experimental diabetes [16] affects the change of the blood plasma refractive index and absorption coefficient, which is

* Presented at the Fundamentals of Laser Micro- and Nanotechnologies (FLAMN-16) International Symposium (Pushkin, Leningrad oblast, 27 June to 1 July 2016).

O.A. Smolyanskaya, O.V. Kravtsenyuk, E.L. Odlyanitskiy, M.K. Khodzitsky ITMO University, Kronverksky prosp. 49, 197101 Saint Petersburg, Russia;
e-mail: smolyanskaya@corp.ifmo.ru; khodzitskiy@yandex.ru;
A.V. Panchenko N.N. Petrov Research Institute of Oncology, Ministry of Healthcare of the Russian Federation, Leningradskaya ul. 68, poselok Pesochnyi, 197758 Saint Petersburg, Russia;
J.P. Guillet Bordeaux University, IMS, UMR CNRS 5218, 351 Cours de la libération 33405 Talence, France;
O.P. Cherkasova Institute of Laser Physics, Siberian Branch, Russian Academy of Sciences, prosp. Akad. Lavrentyeva 13/3, 630090 Novosibirsk, Russia

Received 24 March 2017; revision received 18 September 2017
Kvantovaya Elektronika **47** (11) 1031–1040 (2017)
Translated by V.L. Derbov

particularly strong for the complicated diabetes [17, 18]. Ezerskaya et al. [19] reported that the HL60 and THP1 leucosis cell lines have the factor of scattering anisotropy and the absorption coefficient of THz radiation increased by a few times in comparison with the normal cells.

Thus, the literature analysis shows that such blood components as erythrocytes and thrombocytes, as well as a number of metabolites, contribute to the absorption of THz radiation by blood. However, we could not find publications on the application of THz pulsed spectroscopy to the study of blood and its components in the case of the oncological disease development. In the present paper, we report the experimental studies and numerical simulations aimed at the determination of the most sensitive object for the diagnostics of oncological diseases in the THz frequency region.

We experimentally studied the reflection spectra of the whole blood, the blood plasma, and the suspension of Ehrlich tumour cells. For these samples, the dispersion of the complex permittivity was determined. The measurements were carried out in the frequency range 0.1–1.0 THz in the control group of SHR line mice and similar mice with grafted Ehrlich tumour, which is a convenient and well-studied model of malignant neoplasm [20]. The pathomorphological evaluation of the experimental animals was also performed to exclude the accompanying diseases that could affect the studied parameters.

We simulated the phantom of a biological sample having a complex shape with subsequent modelling of the process of its interaction with THz radiation and determination of its optical characteristics.

The main object of study in the present paper was the blood plasma. It is a yellowish liquid obtained after the separation of blood formed elements and consisting of water (90%) and dissolved substances (10%), including proteins (7%–8%), in particular, albumins, globulins, coagulation factors, as well as organic and mineral compounds [21]. Besides that, the blood plasma contains the dissolved nutritive substances (glucose, lipids), hormones, vitamins, enzymes, intermediate and final products of metabolism and nonorganic substances. Depending on the method of preparation, the experimental sample of blood plasma can contain thrombocytes in different proportion [22], the extracellular bubbles released by cells and having a diameter from 30 nm to 5 μm [23], and the circulating micro-RNA molecules [24]. We also studied a suspension of tumour cells in the 0.9% solution of NaCl (saline). This suspension mainly contains the tumour cells having a size 14–20 μm, but a small amount of other cells (e.g., lymphocytes) can be also present. Note that the size of formed blood elements, blood plasma components, and particles of tumour suspension (from 30 nm to 20 μm) are much smaller than the wavelength of the incident THz radiation (from 300 μm to 3 mm).

2. Object-of-study preparation

The study was carried out with 9 male outbred SHR mice (donors) and 10 female outbred SHR mice (experimental group) 3 months old with the body mass 25–30 g (own breeding, N.N. Petrov Research Institute of Oncology, Saint Petersburg). The animals were kept in standard cages of T2 type in the ventilated vivarium under the standard illumination regime at the temperature 18–22 °C. They received the standard laboratory forage PK120 ('Laboratorkorm', Moscow) and the tap water *ad libitum*.

In the work, we used the strain of the grafted Ehrlich ascites carcinoma of mice (N.N. Petrov Research Institute of Oncology) in the form of a suspension of tumour cells from the abdominal cavity. The curve of the solid tumour growth [20] and the photograph of a mouse on the 14th day of the tumour development are presented in Fig. 1. The tumour grows in the nodal form.

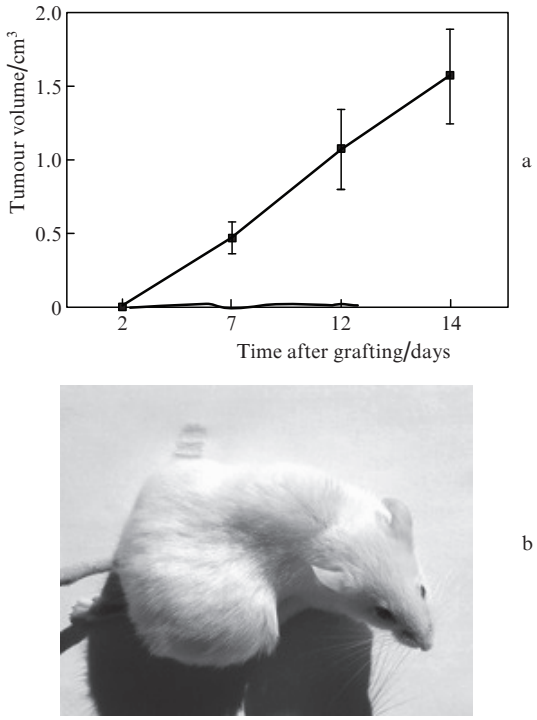

Figure 1. (a) Growth curve of subcutaneous Ehrlich tumour and (b) photograph of a mouse with a large tumour node.

First, we obtained the ascitic liquid from the donor mice with the concentration 5×10^6 tumour cells per 1 mL and then used it to prepare the suspension of tumour cells in the 0.9% solution of NaCl. The suspension was used for the studies in the THz range and for subcutaneous injection to the mice (0.2 mL of the tumour cells suspension in the saline, 10^6 tumour cells per mouse) to develop a grafted nodal tumour (see Fig. 1b).

The suspension of tumour cells was prepared by adding saline to the ascitic liquid in the proportion 1 : 1 with subsequent centrifuging during 5 minutes at 1500 revolutions per minute. We resuspended the sediment in the same solution and centrifuged again, the obtained sediment was again resuspended, and after that, the concentration of cells was counted in the Goryaev chamber using the standard procedure [25].

The evaluation of the tumour growth (Fig. 1a) was performed following the standard technique, namely, the length and the width of the tumour nodes were measured and the tumour volume was calculated using the ellipsoid formula

$$V = ab^2/2, \tag{1}$$

where a is the maximal longitudinal dimension (length) and b is the maximal transverse dimension (width) of the tumour node.

In the end of the experiment (on the 14-th day after the tumour grafting), we performed the pathomorphological examination of the experimental animals with macroscopic evaluation of internals with the purpose to eliminate the accompanying diseases that could affect the studied parameters.

In the studies we used the whole blood and the blood plasma obtained by centrifuging the whole blood during 5 minutes at 1500 revolutions per minute. The blood from the murine tail tips was collected in test tubes with K_2EDTA. The general blood analysis was performed using a Mindray 2800Vet automated haematological analyser (China). The time from the moment of blood sampling until the execution of haematological analysis amounted to one hour. Then the blood samples were transported in a plastic container with a room temperature coolant to perform the spectroscopic studies. The time interval between the sampling of blood from the donor mice and the beginning of studies using a THz spectrometer was about three hours, and the entire measurement (12 test tubes) was finished in eight hours after the blood sampling. During this time, the blood samples were kept in the same test tubes.

The statistical processing of the data was implemented using the 'Statistica 6' applied software package (Statsoft, USA). The results were evaluated using Student's t-test. The probability of the zero hypothesis validity was accepted at the 5% significance level. The data were presented in the form $M \pm m$, where M is the sample mean value and m is the arithmetic mean deviation.

3. Setup for time-resolved THz spectrometry

A series of experiments were performed using the setup generating the broadband THz pulsed radiation by affecting the undoped indium arsenide crystal [26, 27] placed in the permanent magnetic field 2.4 T [28] by femtosecond pulses of a FL-1 laser (the active medium Yb:KYW, λ = 1040 nm, t_{pl} = 46 fs, f = 70 MHz, $P \geqslant 1$W). The generated radiation passes through the Teflon filter cutting off the wavelengths shorter than 50 μm and then is incident on the sample. The sample is fixed in the plane, perpendicular to the optical axis, and the THz radiation experiences diffraction passing through it. The electrooptic detection is implemented by means of a quarter-wave plate, a Wollaston prism, a balance photodetector and a lock-in amplifier [29]. The filtered and amplified signal is transmitted to a computer via an ADC. The error of frequency determination in the measurements amounts to ~10 GHz for the transmission regime and 15 GHz for the regime of THz radiation reflection [30]. The setup is PC-controlled using the NI LabVIEW software environment, which controls the time delay of the probe femtosecond pulse and the measurement process, as well as executes the recording of the terahertz pulse temporal shape.

The schematic of the universal THz pulsed spectrometer is presented in Fig. 2 [31]. The THz radiation used in this experimental setup has the following parameters: the spectral range 0.1–2.0 THz, the mean power ~0.3 μW, and the pulse duration 2.7 ps. The major part of the energy was distributed between 0.1 and 0.6 THz with a maximum near 0.2 THz (Fig. 3b).

The method of measurements in the reflection regime was proposed in [31]. If the THz pulsed radiation is reflected from the silicon plate and the sample on the substrate (Fig. 4), then the photodetector will detect both the pulse of radiation reflected from the silicon plate and the delayed pulse of radiation reflected from the interface between the silicon plate and the sample.

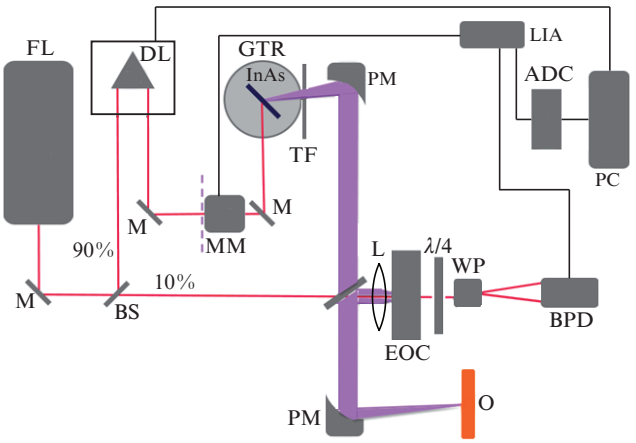

Figure 2. Schematic of a THz spectrometer: (FL) femtosecond laser FL-1; (M) mirror; (BS) beam splitter; (DL) optical delay line; (MM) mechanical modulator; (GTR) generator of THz radiation; (TF) Teflon filter; (PM) parabolic mirror; (L) lens made of TPX plastic; (EOC) electrooptic CdTe crystal; (WP) Wollaston prism; (BPD) balance photodetector; (LIA) lock-in amplifier; (ADC) analogue-to-digital convertor; (O) object of study.

The THz field is recorded as a function of the probe pulse time delay (Fig. 3). The Fourier transform of the THz pulse field allows the determination of its frequency spectrum

$$\tilde{E}(\omega) = A(\omega)\exp[-i\varphi(\omega)] = \frac{1}{2\pi}\int_{-\infty}^{\infty} dt E(t)\exp(-i\omega t), \quad (2)$$

where $\tilde{E}(\omega)$ is the complex amplitude of the signal; $A(\omega)$ is the modulus of the complex amplitude of the signal; and $\varphi(\omega)$ is the phase of the complex amplitude of the signal. Recording the THz pulse field after its interaction with the object of study and then calculating the spectrum by means of Eqn (2), one can obtain the spectral characteristic of the object in the range of frequencies present in the spectrum of the pulse. Since the determination of the spectrum occurs by detecting the field (oscillogram) of the pulse, the method is commonly referred to as terahertz time-domain spectroscopy (THz TDS). A THz pulse usually contains only a few field cycles so that its spectrum can cover more than an octave.

When the pulse passes through a liquid biological sample, its amplitude decreases and the temporal shape and polarisation may change. Since water is a nongyrotropic object, and the objects studied in the present paper contain mainly water, we assume below that the studied samples are nongyrotropic and do not change the polarisation state of the initial THz pulse.

4. Technique of measuring the optical properties of the blood sample and its components using a THz pulsed spectrometer

In order to study the optical properties of the blood sample and its components using a THz pulsed spectrometer we developed the procedure of analysing a liquid sample (blood, blood plasma, suspension of tumour cells) in the reflection regime. The sample of blood or blood plasma was not diluted. Its volume that amounted to 20 μL was measured with micro-

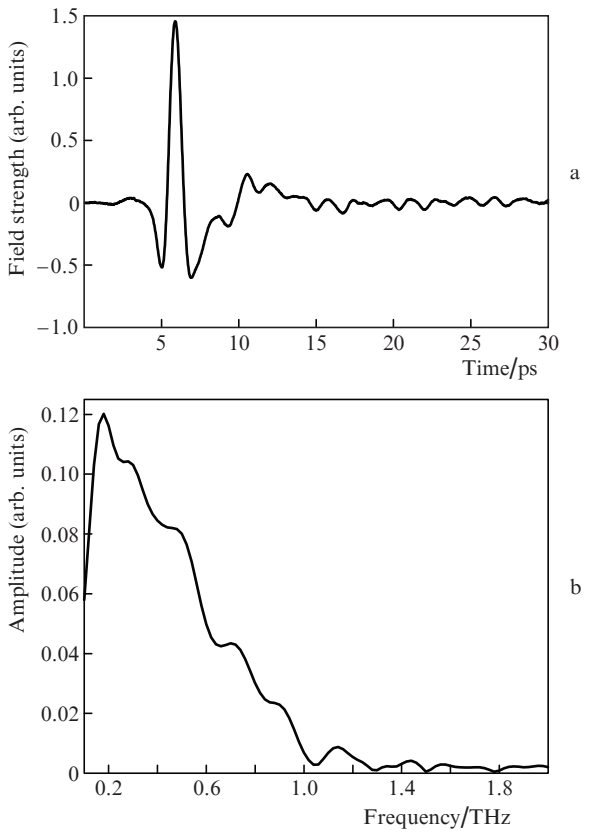

Figure 3. (a) Electric field of the THz pulse and (b) its frequency spectrum for the pulse propagating in the air.

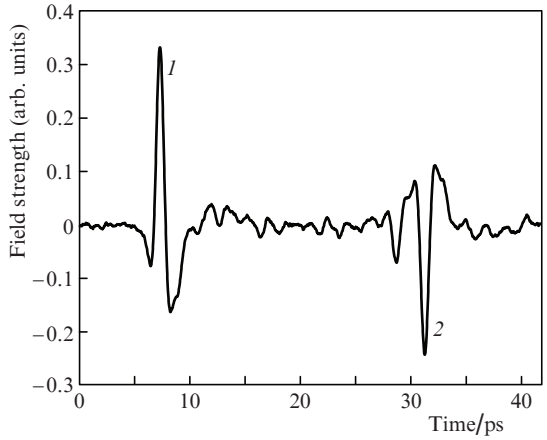

Figure 4. Electric field of the THz pulse reflected (*1*) from the first surface of the silicon plate and (*2*) from the interface between the silicon plate and the sample.

doser after careful mixing of the blood sample during three minutes by overturning the test tube. After that the sample was placed between the plastic plate and the silicon one (the thickness 1.04 mm and $n_{Si} = 3.4$) (Fig. 5), due to which the sample was not dried during the measurements. The diagnostics time for one sample amounted to 2–3 minutes.

The covering silicon plate not subjected to additional compression was used in the experiment for the following reasons. First, biological samples, especially the liquid ones, have different thicknesses at each point of the surface, so that

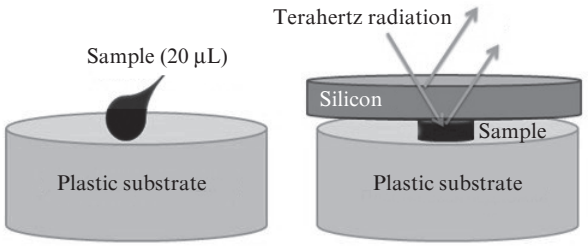

Figure 5. Technique of blood sample preparation for the study using the THz spectrometer.

it is hard to measure the thickness, and the nonplanar outer surface deviates the radiation reflection angle with respect to the value implied by the optical scheme of the experimental setup. Second, the liquid object gets dried, which can essentially modify its spectral properties.

To find the refractive index of the biological object placed under the silicon plate, one has to measure its refractive index n_{Si} and the thickness d_{Si}.

The measurement of the variations of the phase and frequency of the THz pulse temporal shape allows the permittivity of the studied sample to be determined. The ratio of the Fourier transforms of the object signal $[\hat{E}_s(\nu)]$ and the reference one $[\hat{E}_r(\nu)]$ is written as

$$\frac{\hat{E}_s(\nu)}{\hat{E}_r(\nu)} = \frac{t_{aSi}\hat{r}_{Sisam}t_{Sia}}{r_{aSi}}\exp\left(i\frac{4\pi n_{Si}d_{Si}\nu}{c}\right), \tag{3}$$

where t_{aSi}, t_{Sia}, r_{aSi}, and $\hat{r}_{Sisam}$ are the Fresnel coefficients for the transmission (t) and reflection (r) of the normally incident radiation. The subscripts indicate the boundaries separating air (a), silicon (Si), and sample (sam). The Fresnel coefficients for the air–silicon interface are real-valued, since the dry air and the silicon are known not to absorb radiation. The exponent determines the phase shift of the radiation in the course of propagation through the silicon plate. At normal incidence of radiation on the sample, the complex Fresnel reflection coefficient at the silicon–sample interface is presented in the form:

$$\hat{r}_{Sisam} = \frac{n_{Si} - \hat{n}_{sam}}{n_{Si} + \hat{n}_{sam}}, \tag{4}$$

where $\hat{n}_{sam} = n_{sam} + i\alpha_{sam}c/(4\pi\nu)$ is the complex refractive index of the sample. Having expressed the reflection coefficient according to the Euler formula, $\hat{r}_{Sisam} = R\exp(i\theta)$, and solving Eqn (4), we arrive at the expressions for the unknown refractive indices (n_{sam}) and absorption coefficients (α_{sam}) of the sample:

$$n_{sam} = \frac{n_{Si}(1 - R^2)}{1 + R^2 + 2R\cos\theta}, \tag{5}$$

$$\alpha_{sam} = \frac{4\pi n_{Si}\nu}{c}\frac{-2R\sin\theta}{1 + 2R^2 + 2R\cos\theta}. \tag{6}$$

Since for the silicon plate both n_{Si} and d_{Si} are known, the amplitude R and the phase angle θ can be determined from the experimental data by extracting the quantity $\hat{r}_{Sisam} = R\exp(i\theta)$ from Eqn (3). The real and imaginary part of the permittivity $\hat{\varepsilon} = \varepsilon' + i\varepsilon''$ are calculated from the relation $\hat{\varepsilon} = \hat{n}^2$.

Obviously, the optical constants of the samples, obtained from Eqns (5) and (6), possess a strong dependence on the accuracy of the n_{Si} and d_{Si} measurements. Therefore, before each series of measurements the calibration measurement was carried out to determine the characteristics of the silicon plate.

The ratio of the Fourier transforms of the radiation pulses reflected from the air–silicon interface, $\hat{E}_{aSi}(\nu)$, and from the silicon–air interface, $\hat{E}_{Sia}(\nu)$, permits determining the refractive indices of air and silicon, using the expressions, analogous to Eqn (3):

$$\frac{\hat{E}_{Sia}(\nu)}{\hat{E}_{aSi}(\nu)} = \frac{t_{aSi} r_{Sia} t_{Sia}}{r_{aSi}} \exp\left(i \frac{4\pi n_{Si} d_{Si} \nu}{c}\right), \tag{7}$$

where the real-valued Fresnel transmission and reflection coefficients t_{aSi}, t_{Sia}, r_{aSi}, and t_{Sisam} depend only on n_{Si} and n_a (the refractive index of air) for the normal incidence of radiation. If we express $\hat{E}_{Sia}(\nu)/\hat{E}_{aSi}(\nu)$ as $\hat{E}_{Sia}(\nu)/\hat{E}_{aSi}(\nu)$ and make use of the fact that $r_{Sia}/r_{aSi} = -1 = \exp(i\pi)$ for the normal incidence of radiation, then the unknown refractive index n_{Si} can be calculated from the phase part of Eqn (7):

$$n_{Si} = \frac{(\theta_{Sia} - \pi) c}{4\pi d_{Si} \nu}; \tag{8}$$

while the amplitude part of Eqn (7) will yield

$$n_{Si} = \frac{2 - R_{Sia} + 2\sqrt{1 - R_{Sia}}}{R_{Sia}} n_a. \tag{9}$$

Thus, we arrive at two equations, (8) and (9), with two unknowns, n_{Si} and d_{Si}, which allows their calculation using only one measurement.

5. Experimental results and discussion

In our paper [32] it was shown that the THz reflection spectra of whole blood in outbred male and female albino SHR mice are coincident. In the haematological study, in female mice the observed relative and absolute content of granulocytes was smaller, and the content of lymphocytes was somewhat higher; however, these differences of haematological indicators of white blood cells (leucocytes) did not affect the spectral characteristics of whole blood. In Ref. [32] we also studied the influence of different stages of cancer development and chronical inflammation on the spectral characteristics of whole blood. It was shown that in the range from 0.1 to 1.0 THz there are no significant differences in the absorption coefficients and refractive indices of the whole blood samples between the animals from the control group and the animals with the studied pathologies. In the present paper, we performed the comparative analysis of reflection spectra of the whole blood, the blood plasma, and the suspension of Ehrlich carcinoma cells. Figure 6 presents the dispersion of the refractive index and the absorption coefficient, as well as the dispersion of the real and imaginary parts of permittivity of the whole blood and the blood plasma for the control group of animals and the animals with Ehrlich carcinoma (oncological group) in 14 days after the grafting of the tumour.

In the frequency range 0.5–0.6 THz, the refractive index of the whole blood amounts to ~2.09 in the animals of the control group, and to 2.00 in the animals of the oncological group. For the blood plasma, this indicator is equal to 2.20 in the animals of the control group and 2.10 in those of the oncological group in the range of high frequencies (0.7–0.8 THz). In the frequency range 0.6–0.8 THz, the absorption coefficient of the blood plasma in a mouse of control group exceeds this indicator of the blood plasma in an animal with Ehrlich carcinoma by 17%–23% on average. The increase in the absorption index of the animals' blood plasma in the frequency range 0.7–0.8 THz can be due to the absorption by water at the frequency 0.75 THz, reported in Ref. [33]. The comparison of ε' values in the whole blood of the animals from the control and the oncological group (Fig. 6c) has shown that the maximal difference exists in the frequency range 0.5–0.7 THz. For example, at the frequency 0.6 THz the value of ε' for the whole blood of the animals from the control group amounts to ~3.20, and for the oncological group it equals ~2.45. The difference in the values of ε' for the blood plasma of the animals from the control group and the oncological one is maximal in the range 0.55–0.75 THz. In this range of frequencies the real part of the permittivity of blood plasma of an animal with Ehrlich carcinoma exceeds ε' of a mouse from the control group by 17%–39%. The values of the imaginary part of the permittivity ε'' for the whole blood of both groups are sufficiently close to each other. At the same time, the comparison of ε'' for the blood plasma of the animals shows a difference in the ranges 0.3–0.4 and 0.6–0.8 THz. For example, at the frequency 0.7 THz the value of ε'' for the blood plasma of the animals from the control group amounts to 6.60, while for the oncological group it equals ~5.35.

In Ref. [34] using the method of dynamic light scattering in diluted preparations of blood plasma of laboratory animals, described in the present paper, the size distribution of the components was estimated. In this case, the difference in the characteristic size of plasma components was observed. In the animals from the control group, a majority of particles had the diameter from 7 to 40 nm, while in the animals with Ehrlich carcinoma it was from 40 to 90 nm, which significantly exceeds the size of the plasma components in the animals from the control group. Based on these observations, one can suppose that the significant difference in absorption coefficients of blood plasma between the animals from the control group and the oncological one in the THz spectral range can be explained by a significant enlargement of the blood plasma particles with tumour development, giving rise to the reduction of the volume content of water in plasma.

From the above considerations one can draw a conclusion that in the studied THz range of frequencies the absorption by both water and erythrocytes of the whole blood of laboratory animals dominates and does not allow one to get reliable information on the changes in the composition of other blood components. The blood plasma of the animals appeared to be a more representative object for the study using THz radiation.

Figure 7 presents the optical characteristics of the suspension of tumour cells in the 0.9% solution of NaCl, the blood plasma of a mouse with the Ehrlich tumour, and the pure 0.9% solution of NaCl in the THz frequency range. It is seen that in the range 0.3–0.7 THz the refractive index of the saline exceeds the refractive index of this solution with the suspension of oncological cells, while the blood plasma of the animals with developing Ehrlich tumour possesses the lowest refractive index. In the frequency range 0.5–0.7 THz the refractive index of these samples takes the values 2.22, 2.15, and 2.09, respectively. A similar situation in this frequency

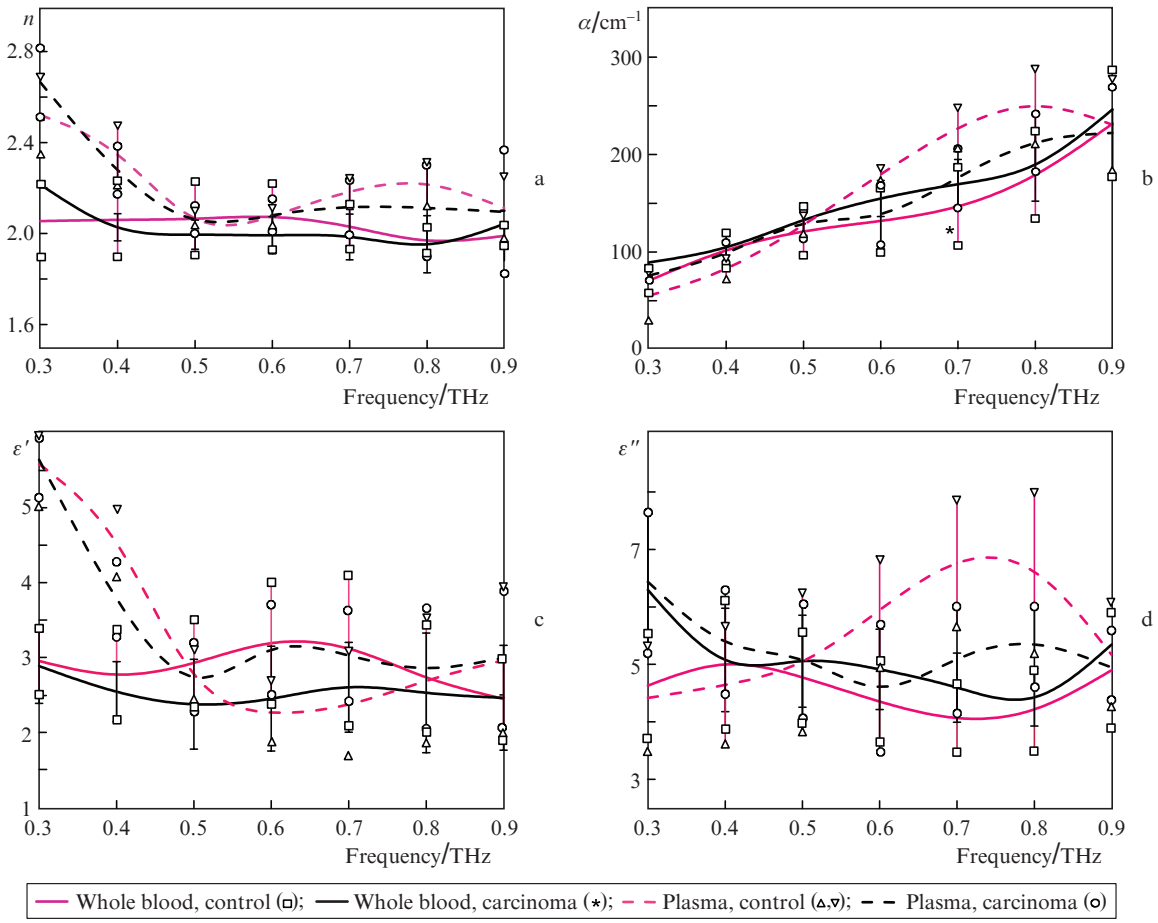

Figure 6. Spectral dependences of the optical characteristics (a) n, (b) α, (c) ε', and (d) ε'' of the whole blood and the blood plasma of the mice from the control group and from the group with Ehrlich carcinoma in the THz frequency range. The symbols denote the boundaries of the arithmetic mean deviation for the frequency dependences of the appropriate optical characteristics of the studied samples. The confidence of the results for the groups 'plasma, carcinoma' and 'plasma control' is $p < 0.05$.

range is observed in these samples for the absorption index, the difference being essentially larger. Thus, at the frequency 0.6 THz, the absorption index of the 0.9% solution of NaCl exceeds the absorption index of the same solution with suspension of oncological cells by 24% on average, while the absorption index of the blood plasma of the animals with Ehrlich carcinoma is greater by 44%. One can see from Fig. 7c that the values of ε' for the 0.9% solution of NaCl and the suspension of tumour cells in the saline have no essential differences. However, in the range 0.5–0.9 THz the values of ε' for blood plasma of the animals from the oncological group are on average by 25% higher than those for the suspension of tumour cells in the 0.9% solution of NaCl and for the saline itself. The dependences of the imaginary part of the permittivity ε'' for the 0.9% solution of NaCl and the suspension of tumour cells in it also demonstrate a similar behaviour. The values of ε'' for the suspension of tumour cells in 0.9% solution of NaCl and for the 0.9% solution of NaCl itself are on average by 45% greater than those for the blood plasma of animals from the oncological group. From these observations, one can draw a conclusion that the presence of tumour cells in the solution of NaCl essentially increases its transmission coefficient for the THz radiation due to the partial replacement of water in the solution with carcinoma cells. One can also suppose that the observed relatively small values of the absorption coefficient of the blood plasma in the animals with Ehrlich carcinoma in comparison with the values of the absorption index for the suspension of tumour cells in 0.9% solution of NaCl are due to even smaller water content in this sample.

The dependences presented in Fig. 8 show that the change in the concentration from 10 to 10^6 tumour cells per 1 mL of saline practically does not change the optical properties of the sample in the studied THz frequency range.

The experimental data obtained in the present work do not provide clear information on the mechanism causing the difference in refractive index and absorption coefficient of blood plasma in the animals from the control group and the oncological one in the terahertz frequency range. On the one hand, the discovered effect could be associated with the fact that the blood plasma in mice with Ehrlich carcinoma, comprising the components (particles) of larger size, contains smaller amount of water as compared to the blood plasma of the mice from the control group. On the other hand, one can assume that this effect can be due to the changes in subcellular structures that appear in mice with Ehrlich carcinoma. The clarification of the issue is possible by performing a numerical experiment simulating the phantom of a biological sample with a complex structure and its optical characteristics in the studied range of frequencies.

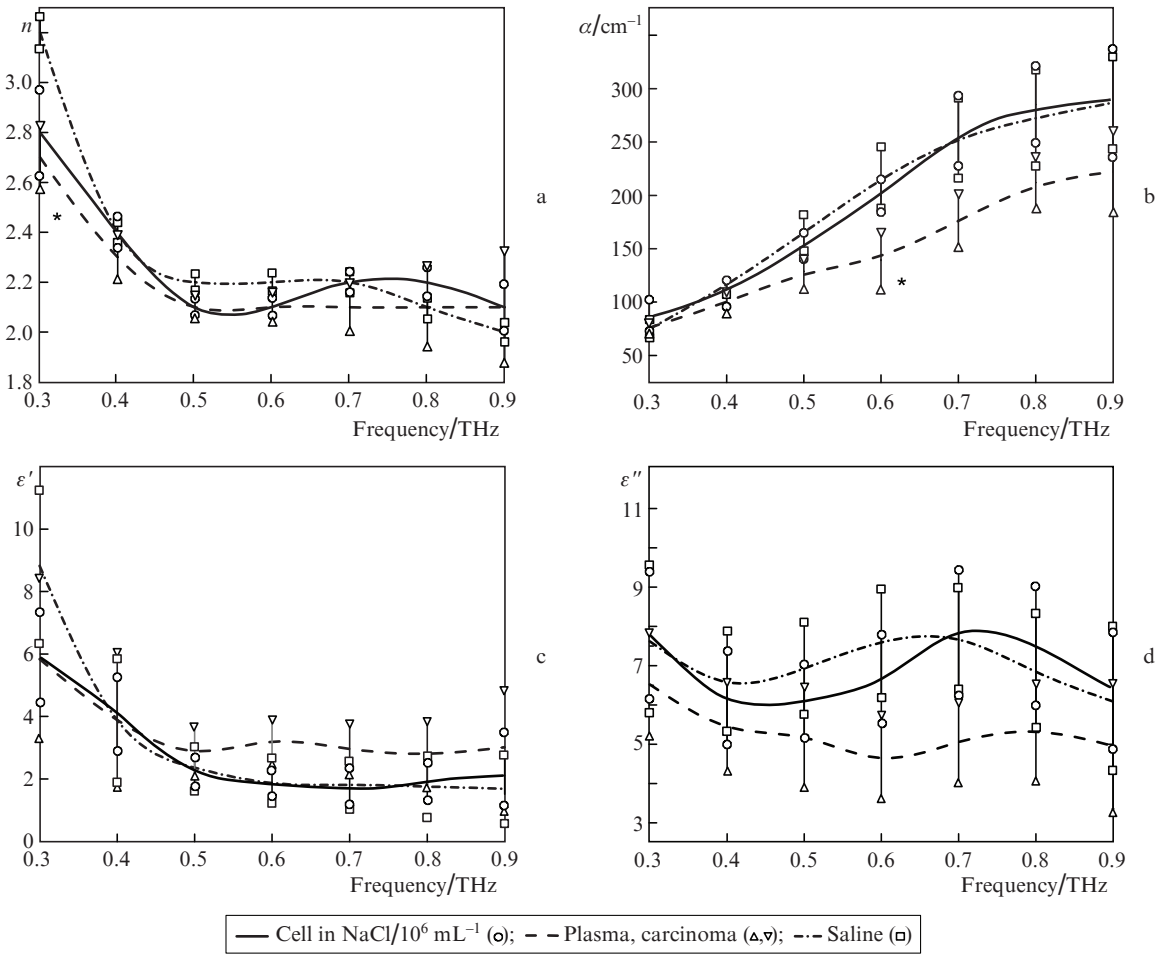

Figure 7. Optical characteristics (a) n, (b) α, (c) ε', and (d) ε'' of the studied samples: the suspension of tumour cells in 0.9% solution of NaCl, the blood plasma of the mouse with Ehrlich carcinoma, and pure 0.9% solution of NaCl in the THz frequency range. The symbols denote the boundaries of the arithmetic mean deviation for the frequency dependences of the appropriate optical characteristics of the studied samples. The confidence of the results for the groups 'plasma, carcinoma' and 'saline' is $p < 0.05$.

6. Numerical modelling of the phantom of a biological object and the procedure of determining its optical characteristics from THz visualisation

In order to elaborate a package of applied software that simulates our experiments on the determination of optical characteristics of biological objects by means of the THz pulsed radiation, we used the finite-difference time-domain (FDTD) method [35]. This method belonging to the class of finite-difference methods for solving differential equations is a simple and efficient tool of three-dimensional numerical modelling of objects of arbitrary shape, with dispersion and nonlinear properties. The method allows the simulation of the process of propagation of electromagnetic radiation through these objects, based on a theoretical model – the finite-difference form of Maxwell's differential equations. The finite-difference calculation is based on the iteration procedure, in which the values of the components at each step are calculated from the values of the components at previous steps. Thus, to perform calculations it is necessary to discretise the domain of the problem into elementary cells and set the initial conditions for all components of the electromagnetic field. To provide an adequate result of the present model operation, the variation of the electromagnetic field near the discrete should be insignificant, i.e., the dimensions of the elementary cell should amount to a few parts of wavelength [35]. We used the grid with hexagonal cells and the Cartesian system of coordinates.

Under the conditions of our experiment, the radiation wavelengths varied from 300 to 3000 μm so that the minimal size of mesh spacing was chosen to be ~0.57 μm and the maximal one 7.49 μm. Since in the future within the frameworks of the formulated problem we suppose to simulate complex objects with an essentially inhomogeneous structure, the variation of the mesh spacing values is necessary to increase the accuracy of calculations in each part of the object volume.

The phantom structure (the object of study) for the numerical experiment and the geometry of experiment are schematically presented in Fig. 9. The modelled biological object was taken in the form of a rectangular parallelepiped about 100 μm high. As phantoms of biological objects for the calibration numerical experiment described in the present paper, we used the following models: 1) the above rectangular parallelepiped with the optical characteristics of saline; 2) the same parallelepiped with the optical characteristics of saline, containing a singular inhomogeneity with the optical characteristics of the blood plasma from the mice with Ehrlich carcinoma. The values of the optical characteristics of refraction and absorption for the 0.9% solution of NaCl and for the blood plasma of mice with Ehrlich carcinoma were taken

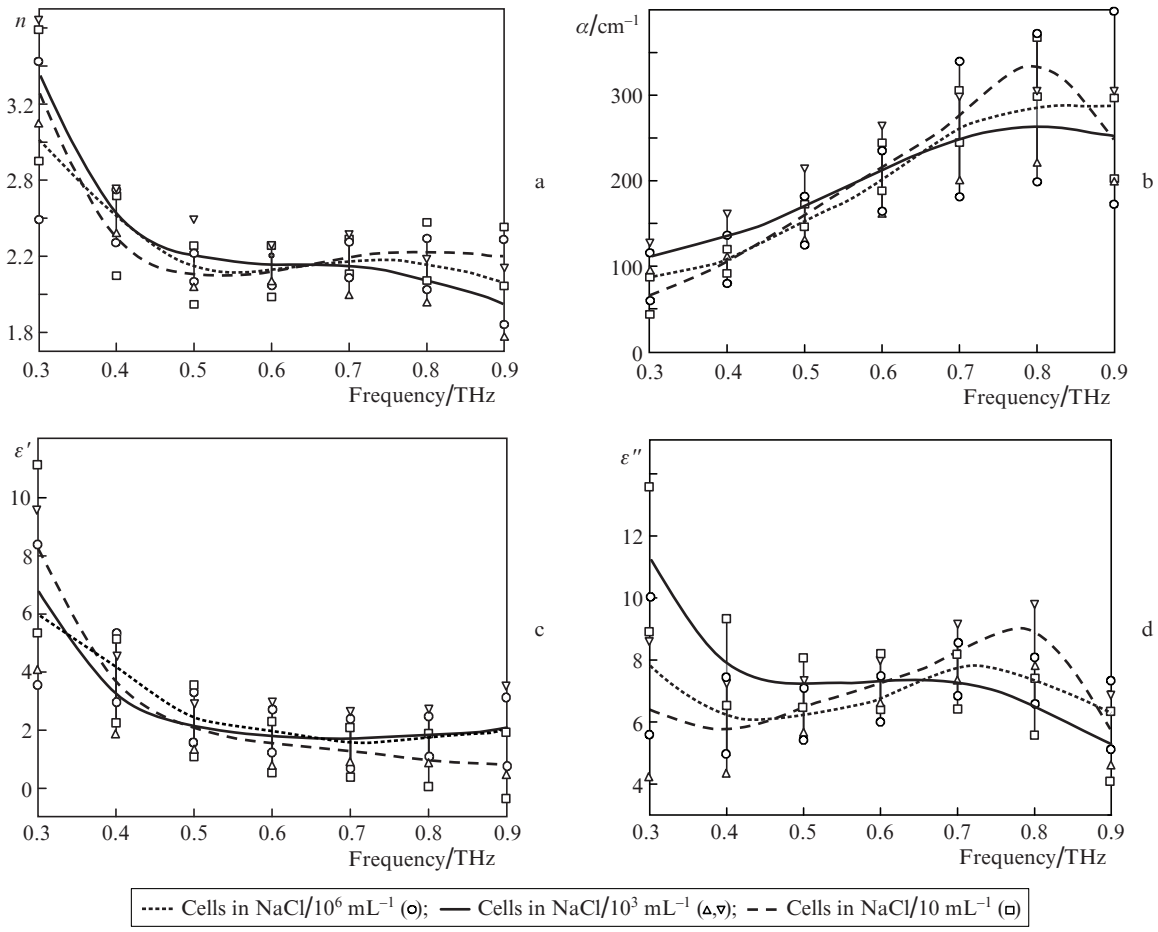

Figure 8. Optical characteristics (a) n, (b) α, (c) ε', and (d) ε'' of the suspension of tumour cells in 0.9% solution of NaCl with different concentration of the cells. The symbols denote the boundaries of the arithmetic mean deviation for the frequency dependences of the appropriate optical characteristics of the studied samples.

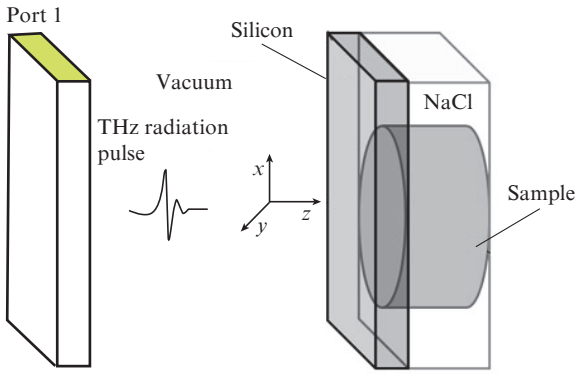

Figure 9. Geometry of the numerical experiment on modelling the characteristics of the scattered electromagnetic wave. The structure of the phantom (the object of study) is a rectangular parallelepiped having the height 100 μm with the optical characteristics of saline, containing a singular cylindrical inhomogeneity with the optical properties of the studied samples.

from the results of the experiment described above in the present paper. As in real experiment, the modelled biological sample was covered from above with a silicon plate ($n_{Si} = 3.4$, the thickness 1.04 mm).

The numerical experiments simulate the solution of the problem when a plane electromagnetic wave with the frequency 0.1–1.0 THz is incident on the silicon–biological sample structure, placed in an infinite space. A source–detector (port 1 in Fig. 9) is placed in front of the structure. Between the silicon plate and the detection port, there is a vacuum layer 1 mm thick. The modelling of the reflected electromagnetic wave characteristics is performed at the silicon–biological sample interface ($z = 0$).

Figure 10 presents the results of numerical modelling of the complex amplitude of the reflected wave signal at frequencies 0.7 and 0.8 THz. It is seen that the shapes of the THz pulse found in the real experiment and in the numerical one are in good agreement. Thus, at the 14th picosecond the reflection from the first surface of the silicon plate, and at the 42th picosecond the reflection from the interface between the silicon plate and the plasma-carcinoma sample is observed.

Figure 11 shows that the reflection coefficients of the studied sample (the blood plasma of a mouse with Ehrlich carcinoma) obtained in the numerical experiment agree well with those of the real experiment in the range 0.5–0.8 THz.

From Fig. 12 one can clearly see that the amplitude of the wave reflected from the surface of saline is very small (Fig. 12a). In the case of the wave incident on the object surface in the region of the cylindrical inclusion having the opti-

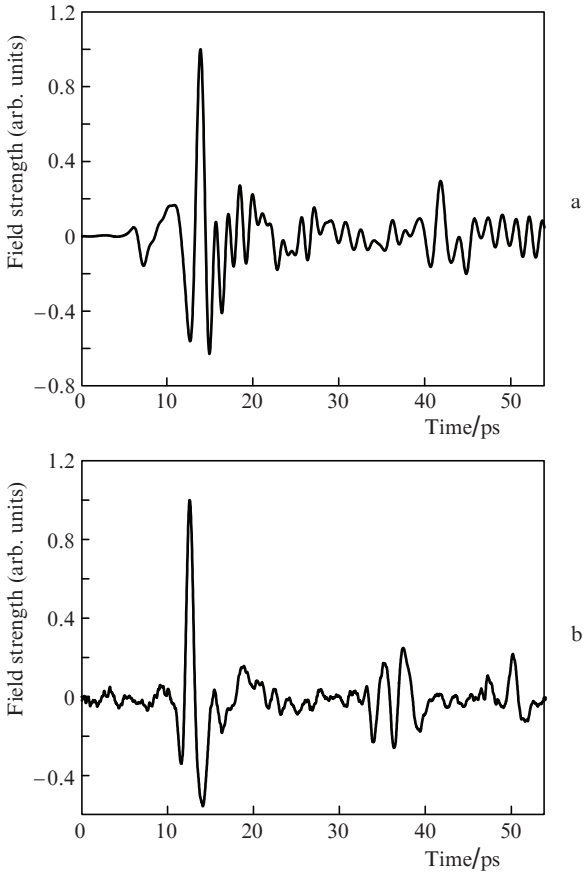

Figure 10. THz pulse fields reflected from the first surface of the silicon plate and from the interface between the silicon plate and the plasma-carcinoma sample: (a) the result of modelling, (b) the experimental result.

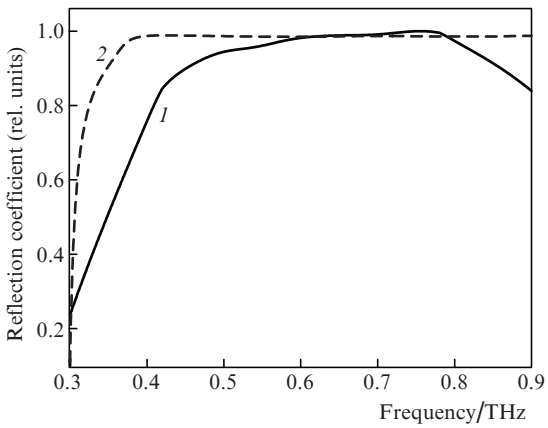

Figure 11. Coefficients of THz signal reflection from the sample with the blood plasma of a mouse with Ehrlich carcinoma, obtained in (*1*) the numerical and (*2*) real experiment.

cal properties of the blood plasma of a mouse with Ehrlich carcinoma, the reflected signal essentially increases (Figs 12b and 12c). In this case, the value of the normalised amplitude modulus of the wave with the frequency 0.8 THz noticeably exceeds the analogous value for the wave with the frequency 0.7 THz, which coincides with the obtained experimental data (see Figs 6 and 7).

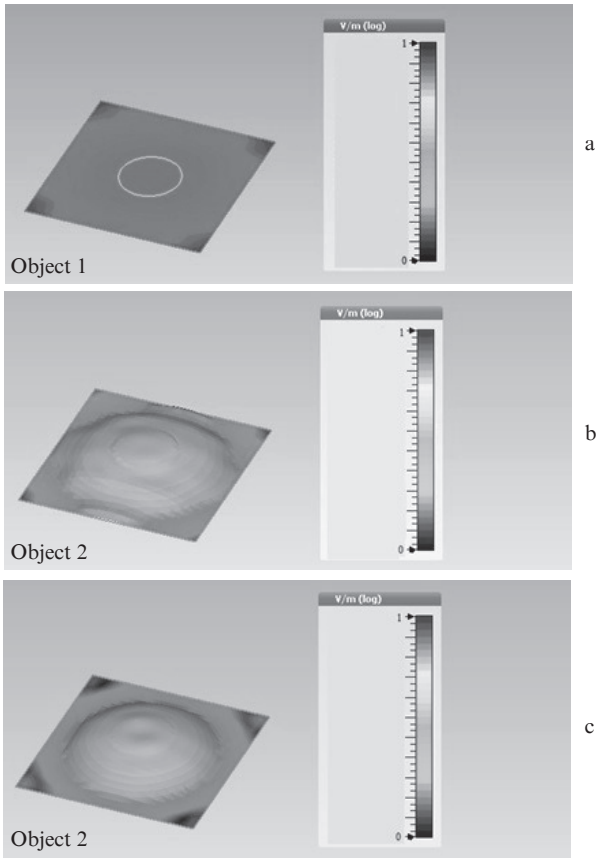

Figure 12. Results of numerical modelling of the amplitude modulus of the wave reflected from the biological object phantom: (a) the frequency 0.7 THz, object 1 with the optical characteristics of the 0.9% solution of NaCl; (b) the frequency 0.7 THz, object 2 with the optical characteristics of 0.9% solution of NaCl and the inhomogeneity with the optical properties of the blood plasma of a mouse with Ehrlich carcinoma; (c) the frequency 0.8 THz, object 2 with the optical characteristics of 0.9% solution of NaCl and the inhomogeneity with the optical properties of the blood plasma of a mouse with Ehrlich carcinoma. The presented values of the reflected wave amplitude modulus are normalised to the amplitude modulus of the incident wave at the appropriate frequency.

Thus, the possibility of using the pulsed THz visualisation in the reflection regime for the express diagnostics of oncological diseases due to the difference in the amplitudes of the signals reflected from the samples from the animals of the control and the oncological groups is shown.

7. Conclusions

Summarising the data of recent publications in the field of THz spectroscopy of the animal and human whole blood, as well as the data obtained by us, we can conclude that such formed blood elements as erythrocytes and thrombocytes make the major contribution to the blood absorption. In this relation, the changes in the composition of other blood elements (lymphocytes and leucocytes) cannot be reliably detected in the whole blood using the methods of THz spectroscopy. As shown by our experiments, the blood plasma is the most promising object of study, since the change of composition caused by pathological processes in the organism can considerably affect the optical properties of the blood plasma of humans and animals in the THz frequency range.

In the present *in vitro* experiment, we revealed the reduction of the amplitude of the absorption coefficient of blood plasma from mice with grafted Ehrlich carcinoma. This observation offers the possibility of developing express diagnostics of oncological diseases using the method of THz pulsed spectroscopy of blood plasma samples. The experimental data obtained in the present work do not provide clear information about the origin of the difference in the absorption indices and reflection coefficients of the blood plasma of the animals from the control group and from the oncological one in the THz frequency range. On the one hand, the discovered effect could be associated with the fact that the blood plasma of mice with Ehrlich carcinoma containing enlarged components (particles) contains smaller amount of water as compared to the blood plasma of the mice from the control group. On the other hand, one can assume that the effects can be due to the changes in subcellular structures, arising in the mice with Ehrlich carcinoma. To clarify this issue we plan further in vitro experiments.

To help the interpretation of the experimental measurements, we elaborated an applied software package that simulates a phantom of biological sample having a complex structure and allows one to simulate numerically the process of THz radiation propagation in this sample and to determine its optical constants. The performed numerical experiment has shown the possibility of visualising the amplitude modulus of the wave reflected from the sample of blood plasma of animals with Ehrlich carcinoma. Good agreement with the experimental data is achieved.

Acknowledgements. The work was carried out under the State Financial Support for Leading Universities of the Russian Federation (Subsidy No. 074-U01).

References

1. Martynov S.A. *Ginekologiya*, **16** (4), 63 (2014).
2. Alekseeva M.L., Gusarova E.V., Mullabayeva S.M., Ponkratov T.S. *Problemy Reproduktsii*, **3**, 65 (2005).
3. *Terahertz Biomedical Science and Technology*. Joo-Hiuk Son (Ed.) (New York: CRC Press, 2014) p. 377.
4. Rønne C., Thrane L., Åstrand P.-O., Wallqvist A., Mikkelsen K.V., Keiding S.R. *J. Chem. Phys*., **107**, 5319 (1997).
5. Ladanyi B.M., Skaf M.S. *Annual Rev. Phys. Chem*., **44** (1), 335 (1993).
6. Zaytsev K.I., Chernomyrdin N.V., Kudrin K.G., Gavdush A.A., Nosov P.A., Yurchenko S.O., Reshetov I.V. *J. Phy*s., **735**, 012076 (2016).
7. Mounaix P., Balacey H., Al-Ibadi A., Macgrogan G., Guillet J.P., Pickwell-MacPherson E. *Proc. 41st Intern. Conf. Infrared, Millimeter, and Terahertz Waves* (Copenhagen, Denmarc, 2016) pp 1–2.22.
8. Doradla P. et al. *J. Biom. Opt*., **18** (9), 090504 (2013).
9. Rong L. et al. *Sci. Rep*., **5**, 8445 (2015).
10. Yookyeong Carolyn Sim, Kang-Min Ahn, Jae Yeon Park, Chan-Sik Park, Joo-Hiuk Son. *IEEE J. Biom. Heal. Inf*., **17** (4), 779 (2013).
11. Yamaguchi S., Fukushi Y., Kubota O., Itsuji T., Ouchi T., Yamamoto S. *Sci. Rep*., **6**, 30124 (2016).
12. Reid C., Reese G., Gibson A.P., Wallace V.P. *IEEE J. Biom. Heal. Inf*., **17** (4), 774 (2013).
13. Jeong K., Huh Y.-M., Kim S.-H., et al. *J. Biom. Opt*., **18** (10), 107008-1 (2013).
14. Angeluts A.A., Balakin A.V., Evdokimov M.G., Ozheredov I.A., Sapozhnikov D.A., Solyankin P.M., Shkurinov A.P., Esaulkov M.N., Nazarov M.M., Cherkasova O.P. *Quantum Electron*., **44** (7), 614 (2014) [*Kvantovaya Elektron*., **44** (7), 614 (2014)].
15. Tzu-Fang Tseng, Borwen You, Hao-Cheng Gao, Tzung-Dau Wang, Chi-Kuang Sun. *Opt. Expess*, **23** (7), 9440 (2015).
16. Cherkasova O.P., Kuznetsova N.V., Pal'chikova N.A., Selyatitskaya V.G. *Diabetes Mellitus*, **14** (2), 37 (2011).
17. Cherkasova O.P., Nazarov M.M., Smirnova I.N., Angeluts A.A., Shkurinov A.P. *Phys. Wave Phen*., **22** (3), 185 (2014).
18. Cherkasova O.P., Nazarov M.M., Angeluts A.A., Shkurinov A.P. *Opt. Spectrosc*., **120** (1), 50 (2016) [*Opt. Spektrosk*., **120** (1), 59 (2016)].
19. Ezerskaya A.A., Serebryakova M.K., Nazarova I.V., Smolyanskaya O.A. *Phys. Wave Phen*., **22** (3), 216 (2014).
20. Anisimov V.N. et al. *Cell Cycle*, **9** (1), 188 (2010).
21. Rumyantsev A.G., Agranenko V.A. *Klinicheskaya transfuziologiya* (Clinical Transfusiology) (Moscow: Geotar-Meditsina, 1997).
22. Hosnuter M., Aslan C., Isik D., Caliskan G., Arslan B., Durgun M. *J. Plast. Surg. Hand. Surg*., **51** (4), 235 (2016).
23. Cvjetkovic A., Lötvall J., Lässer C. *J. Extracell Vesicles*, **3**, 23111 (2014).
24. Xiao-Hui Zheng, Cui Cui, Xin-Xi Zhou, Yi-Xin Zeng, Wei-Hua Jia. *Chin. J. Cancer*, **32** (12), 667 (2013).
25. Ronin V.S. *Rukovodstvo k prakticheskim zanyatiyam po metodam klinicheskikh laboratornykh issledovaniy* (A Manual for the Practical Studies of Methods of Clinical Laboratory Examinations) (Moscow: Meditsina, 1989) p. 161.
26. Gurtler A., Winnewisser C., Helm H., Jepsen P.U. *J. Opt. Soc. Am*., **17**, 74 (2000).
27. Izumida S., Ono S., Liu Z., et al. *Appl. Phys. Lett*., **75**, 451 (1999).
28. Mittleman D.M., Cunningham J., Nuss M.C., Geva M. *Appl. Phys. Lett*., **71**, 16 (1997).
29. Lee Y.S. *Principles of Terahertz Science and Technology* (New York: Springer Science & Business Media, 2009) p. 40.
30. Chan W.L., Deibel J., Mittleman D.M. *Rep. Prog. Phys*., **70**, 1325 (2007).
31. Balbekin N.S., Grachev Ya.V., Smirnov S.V., Bespalov V.G. *J. Phys*., **584**, 012010 (2015).
32. Panchenko A., Tyndyk M., Smolyanskaya O., Sulatskiy M., Kravtsenyuk O., Balbekin N., Khodzitsky M. *J. Phys*., **735** (1), 012081 (2016).
33. Antsygin V.D., Mamrashev A.A., Nikolaev N.A., Potaturkin O.I. *Optoelectron. Instrum. Data Process*., **46** (3), 294 (2010) [*Avtometriya*, **46** (3), 110 (2010)].
34. Chigrin R.N., Andreeva N.V. *J. Phys.: Conf. Ser.*, **737** (1), 012055 (2016).
35. Samarskii A.A., Nikolaev E.S. *Metody resheniya setochnykh uravneniy* (Methods For Solving Finite Difference Equations) (Moscow: Nauka, 1978).